PV-Supercapacitor Tri-port Converter for Frequency Response Services

Sivakrishna Karpana
Department of Electrical Engineering
IIT Kharagpur
Kharagpur, India
karpanasivakrishna@gmail.com

Efstratios Batzelis
School of Electronic and Computer Science
University of Southampton
Southampton, UK
e.batzelis@soton.ac.uk

Suman Maiti
Department of Electrical Engineering
IIT Kharagpur
Kharagpur, India
sumanmaiti@gmail.com

Chandan Chakraborty
Department of Electrical Engineering
IIT Kharagpur
Kharagpur, India
chakraborty@ieee.org

***Abstract*—Frequency Response Services (FRS) have taken a special space among the family of ancillary services required for the stability of the Power Systems (PS). Falling of system inertia, being the inherent capability of the classical rotating generator-based PS, has become a serious concern with the increase in inertia-less renewable energy sources like solar PV Systems (PVS). Hence, it draws the attention of the research community on how to emulate equivalent response from the PVS, either the existing ones or the future installations. Additional Energy Storage (ES) plays a vital role in providing Synthetic Inertia (SI) to the PVS. Super-capacitor (SC) has taken unique stand among the existing ESs due to its faster response, burst power handling capability, and longer life cycle. In this paper, a novel single magnetics (Inductor) based compact, non-isolated Tri-Port Converter (TPC) has been proposed. This allows the designer to integrate a low voltage SC unit to the PVS without the need of a high gain converter. The aim is to emulate SI in the grid connected PVS to provide the major FRS to the PS such as Inertial Response (IR) and Primary Frequency Response (PFR). Finally, the proposed TPC and the implemented control is verified via simulations in MATLAB/SIMULINK.**

Keywords—PV-SC TPC, Supercapacitor, Synthetic Inertia, Inertial Response, Primary Frequency Response, PV systems, triport converter.

I. INTRODUCTION

Unlike the conventional synchronous generator based thermal and hydro power plants, the converter/inverter interfaced renewable energy systems, such as the solar PVS, do not have inherent mechanical inertia. The increasing deployment of new PVS [1] along with the replacement of existing traditional rotating generators is rapidly decreasing the corresponding inertia of the PS, estimated to fall by 22% by the end of 2022 in India [2]. This may lead to serious risk to the stability and reliability of the PS if appropriate measures are not carried out in time. In the traditional PS, the IR is inherent due to kinetic energy stored in the mechanical rotating part of the synchronous machines. Therefore, in case of frequency disturbances due to sudden mismatch of generation and load, the IR is intrinsic in limiting the Rate of Change of Frequency (RoCoF). This is later followed by a slower governor response (primary frequency response) to contain the frequency drop and initiate the process of restoration to the nominal levels.

However, due to rapid increase in solar PV integration and the proportionate fall in the conventional generation, the system is moving towards a state, where a small load and/or generation disturbances may lead to large frequency fluctuation. If it exceeds the standard boundaries set by the national and international grid codes, it may trigger domino disconnections that can lead to load shedding or even system collapse if not managed properly. Looking back to history, many such cases are experienced in different parts of the world. Those incidents were result of either lower frequency nadir, high RoCoF or longer frequency events etc. [2]-[4].

Therefore, it is essential for the PVS to emulate similar or better IR characteristics to synchronous generators to maintain the stability of the PS towards the safer side. To make this possible, additional storage is required. Various kinds of storage types have been used for such applications in literature [5], such as Battery Energy Storage (BES) [6], [7], Superconductive Magnetic Energy Storage (SMES) [8], [9] etc. Apart from that, hybrid energy storage is also found in literature such as PV with Flywheel ES [10] and PV-Diesel-Fuel Cell based hybrid ES [11] etc. as a solution towards larger footprint (installation area) of BES and SMES. Some researchers also have come with the concept of Virtual Energy Storage (VES), where they earmark a portion of PV array's capacity as active power storage, which is also known as PV reserves, power headroom or PV delta power control method [12], [13], which suffers from unavailability of the storage during the night time and larger foot print etc. Under the idea of VES, researchers in [14], [15] used the stored energy in the DC link capacitor and proposed various DC link voltage control techniques to provide SI to the PVS. However, this became less popular due to the demand of a larger capacitor bank, slow dynamic response and lower utilization factor.

Recently, the technology of Ultra-capacitor/ Electric Double Layer Capacitor, commonly known as SC, is gaining popularity among the storages classes due to its faster response, burst power handling capability, and longer life cycle. Although SC shares similar advantages of SMES, it has a much smaller footprint compared to SMES. However, due to its comparatively low energy density, multiple works have been cited using SC as a hybrid storage along with either BES [16] or fuel cell [17] mostly for high-energy intensive applications. Nevertheless, for the low-energy high-power requirements of FRS, the SC could be a very cost-effective option to hybridise a PVS with the needed energy storage. Therefore, this paper focuses on this technology.

Selection of topological configuration is also equally important while integrating ES to a PVS. The most common parallel integration approaches become less appropriate [18], due to the demand of either larger ES with a simple low gain topology or a very high gain complex isolated topology to integrate low voltage ES to the DC link. This is of particular importance for the SC module, which has relatively low and variable terminal voltage. Series/cascaded configuration, as cited in [18], can be a solution to deal with high gain issues while integrating a low voltage ES to the PVS. However, both series and parallel configurations suffer from the drawbacks of larger footprint, higher number of components and low reliability due to the need of an additional interfacing converter for ES.

978-1-6654-5566-4/22/$31.00 ©2022 IEEE

As a more compact approach, many multiport converter topologies are also cited in literature [19]-[29] to optimize the total converter count for PVS, however, with certain limitations like demand of either a high voltage-based ES [19]-[21] or more complex topologies either with galvanic isolation [22], [23], coupled inductor [24], [25] and/or multiple magnetic/capacitive elements based [26]-[28]. To this day, no such multiport configuration is there that incorporates SCs and PV arrays in a compact manner. To cover this gap, the authors here have proposed a TriPort Converter (TPC) Topology to integrate SCs or any other low-voltage ES to PVS for high-power services like FRS. The proposed TPC is not only compact in terms of fewer magnetics and/or switches, but also allows the designer to utilize the SC to the full of its capacity.

The paper is organized into following sections. Section II gives a detailed description of the proposed TPC and its working principle, followed by Section III, which explains the proposed implemented control. In Section IV, the sizing of the SC for FRS is briefed. The idea is validated via MATLAB/Simulink simulations in Section V. Eventually, Section VI concludes the paper.

II. PROPOSED PVSC TPC

A. System Under Considertion

The various ratings of the PVS under consideration and the parameters associated with the targeted/benchmark frequency disturbance profiles for FRS is set out in Table 1.

B. Proposed PVSC-TPC and its Working Principle

The circuit diagram of the proposed PV-SC TPC is shown in the Fig. 1(a). As depicted, it is a Boost derived cascaded topology. The major advantages of the proposed TPC are its compactness and simple topological configuration. This single-magnetics TPC allows the designer to integrate a comparatively very low voltage SC in series with the PV with a just few additional switches to the conventional Boost converter. The various modes of operation of the proposed TPC to understand the current flow path for charging and discharging of SC are shown in Fig. 1(b) to (f) respectively.

During normal operation, when there are no frequency events, the SC should be in idle state and only the available PV power should be delivered to the grid. This can be understood from Fig. 1 (b) and (f), indicating the current flowing path during charging and discharging of the inductor respectively, same as the normal Boost converter operation.

TABLE I. SYSTEM UNDER CONSIDERATION

Targeted system and Frequency fluctuations	Parameters and values
PV System	PV side: 10 kWp, 425 V & 23.5 A DC Link: 700 V AC side: 3Phase VSI, 10 kVA, 400 V (L-L rms) & 50 Hz
Maximum range of continuous frequency fluctuation across nominal frequency	± 0.03 PU (± 150 mHz)
Benchmark PFR profile	Duration: 16.1 sec Frequency nadir: 49.45 Hz Settled frequency: 49.8 Hz.

However, during a frequency distortion, for the discharging of the SC, there could be four possible modes of operations based on the ON/OFF status of the SC discharging switch (S_d) and the switch meant for PV MPPT operation (S_{pv}). For the duration when both S_d and S_{pv} are ON as shown in Fig. 1(c), both PV and SC come in series and charge the inductor. If S_d turns OFF before S_{pv}, then only PV charges the inductor like regular boost mode as shown in Fig. 1(b). On the contrary, If S_{pv} turns OFF before S_d, then the inductor discharges to the DC link via both PV and SC in series as shown in Fig. 1(d). Finally, when S_d turns OFF, the inductor discharges to DC link only through PV like regular boost mode as shown in Fig. 1(f). It may happen that S_d is ON for the entire switching cycle skipping the regular boost modes of operation. Likewise, the charging of the SC has three steps. First, the inductor is charged through PV as shown in Fig. 1(b). This is followed by the charging of the SC when a part of the stored energy of the inductor is diverted to SC for the duration when S_c turns ON after S_{pv} turns OFF as shown in Fig. 1(e) (same as regular Buck-Boost converter). Eventually, when S_c turns OFF, the inductor completely discharges to the DC link as per the current path in Fig. 1(f). The additional two diodes D_c and D_{pv} avoid short circuiting of the PV and/or SC when the switches S_{pv} and/or S_d are ON respectively.

III. CONTROL SCHEME

This section gives a clear-cut idea about the implemented control for the simultaneous manifestation of both the PV MPPT as well as the implementation of the SC power contribution for both IR and PFR altogether. In addition, a

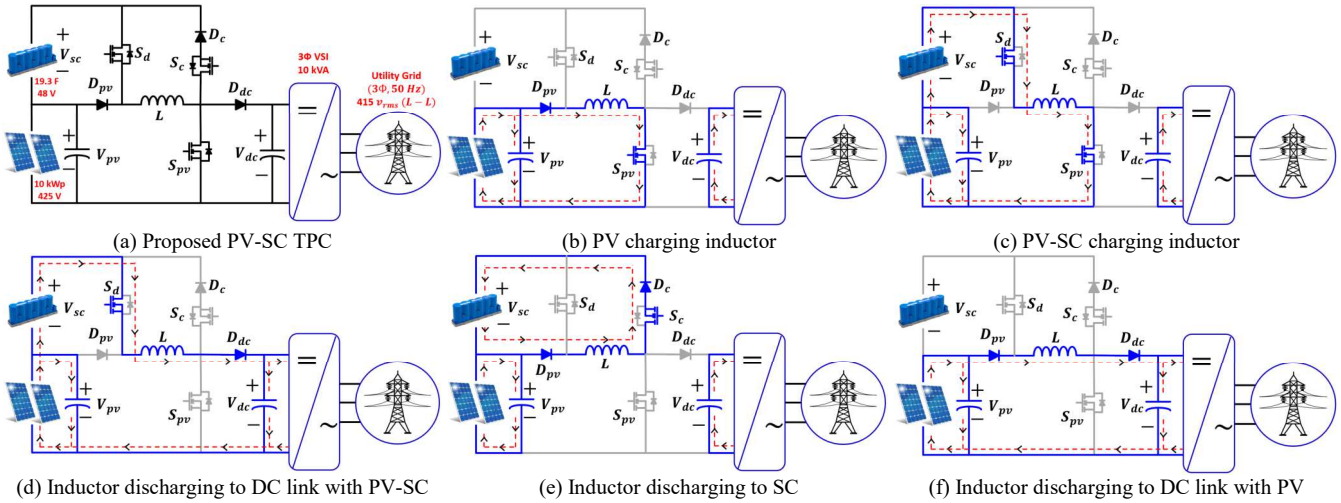

(a) Proposed PV-SC TPC (b) PV charging inductor (c) PV-SC charging inductor

(d) Inductor discharging to DC link with PV-SC (e) Inductor discharging to SC (f) Inductor discharging to DC link with PV

Fig. 1. Proposed PVSC TPC and its working principle.

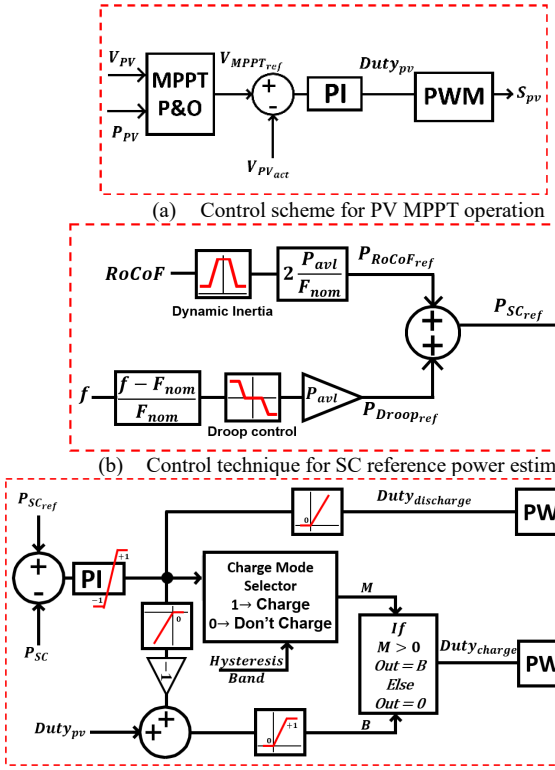

(a) Control scheme for PV MPPT operation

(b) Control technique for SC reference power estimation

(c) Proposed control technique for SC charge/discharge regulation

Fig. 2. Implemented control scheme for both PV MPPT and SC charge/discharge control.

single PI controller control scheme is proposed for the charge/discharge control of the SC. As shown in Fig. 2(a), a standard P&O MPPT algorithm generates $D_{S_{pv}}$, which is further given to PWM block to generate pulses for the main switch S_{pv} to track the PV MPP. The reference SC Power ($P_{SC_{ref}}$) is estimated as per Fig. 2(b), using the common control scheme for both IR and PFR using the concept of dynamic inertia and droop control method explained in [18]. $P_{SC_{ref}}$ is then used to generate appropriate PWM pulses for the switches S_c and S_d to charge and discharge the SC respectively using a novel single PI controller control scheme. As shown in Fig. 2(c), the PI control block takes the error between $P_{SC_{ref}}$ and actual SC power (P_{SC}) as input. Based on the sign and magnitude of the PI output, the appropriate charge/discharge duty for the respective switches is determined via a sequence of saturation blocks and conditional blocks. A hysteresis band helps in avoiding undesirable mode transitions at the verge of charging and discharging of SC due to control dynamics.

The inverter side control is accomplished by using the conventional concept of d-q frame of reference to achieve DC link voltage regulation and PQ control [18].

IV. SIZING OF SC FOR FRS

This section facilitates understanding the methodology adopted for sizing the ES to meet the energy and power demand for the targeted FRS. A few considerations have been taken into account while finalizing the rating of the SC and are enumerated below:

- The net energy demand by SIR acting upon the steady-state continuous frequency fluctuation is nearly zero over a specific period of time. Hence, the maximum energy rating of the SC $E_{SC_{max}}$ should be decided based on the energy demanded by the PFR, rather than SIR.
- Instantaneous power demand by both SIR as well as droop control is expected to be intensive. That is the reason the maximum power demanded by the SC ($P_{SC_{max}}$) should be decided based on the power needs during both continuous frequency fluctuation as well as under frequency events.
- The serial connection of SC with PV limits the discharging capability of the SC to the available PV current ($I_{PV_{avl}}$). Hence $P_{SC_{max}}$ is strictly a function of available PV power ($P_{PV_{avl}}$) if the minute variation in the PV voltage is neglected due to change in solar irradiance.

Along with the above considerations, the authors here have adopted the dynamic inertia emulation technique introduced in [18], as shown in Fig. 3(a). The addition in this paper is that we normalize the SIR contribution ($P_{SC_{SIR}}$) to the available PV power ($P_{PV_{avl}}$) as shown in Fig. 3(b). In that sense, the SIR of the system is proportional to the solar generation output at any time. This indicates that the highest $P_{SC_{SIR}}$ value is attained at 1000 W/m^2 solar insolation and can be verified mathematically as 1046 Watts using (1) [18] for the study-case system.

$$|P_{SC_{SIR}}| = \left|\frac{[RCF_L H_L - RCF_H H_H]^2 P_{PV_{avl}}}{2(H_L - H_H)(RCF_H - RCF_L)F_{nom}}\right| = 1046\ Watts \quad (1)$$

Where, F_{nom} is the nominal system frequency, RCF_L and RCF_H are the minimum and maximum values of RoCoF, and H_L and H_H are the lowest and uppermost values of inertia constant (Table II).

Similarly, the worst-case power demand due to PFR ($P_{SC_{PFR}}$) can be calculated considering only droop control for simplification [18]. The $P_{SC_{PFR}}$ corresponding to the benchmark under-frequency event parameterized in Table I is calculated to be 667 Watts using (2) [18].

$$P_{SC\,PFR} = \frac{P_{PV_{avl}}(F_{nom} - db_{UF} - f_{nadir})}{F_{nom} k_{UF}} = 667\ Watts \quad (2)$$

Where, db_{UF} is the dead band for the droop control, k_{UF} is the droop coefficient and f_{nadir} is the frequency nadir (Table II).

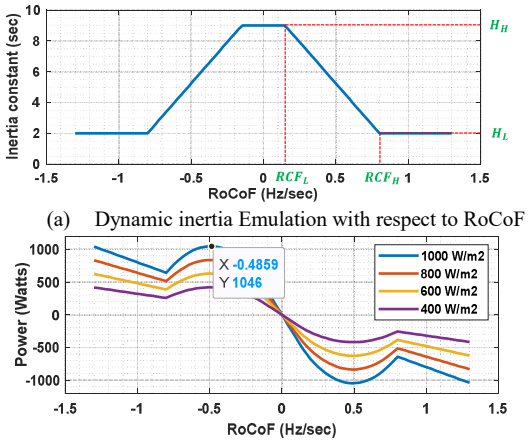

(a) Dynamic inertia Emulation with respect to RoCoF

(b) Demand in SC power with change in solar insolation

Fig. 3. Maximum power demand calculation based on Dynamic Inertia emulation method as a function of available PV power.

TABLE II. DESIGN SPECS UNDER CONSIDERATION

Various design constraints	Parameters and values
Related to RoCoF control	$RCF_L = 0.15\ Hz/sec,\quad RCF_H = 0.15\ Hz/sec, H_L = 2\ secs, H_H = 9\ secs.$
Related to Droop control	$db_{UF} = 0.15\ Hz, k_{UF} = 12\ \%.$

The above constraints for both RoCoF control and droop control are strictly in the hand of the designer and/or subjective to local grid codes. Now, the final selection $P_{SC_{max}}$ will be the maximum of both $P_{SC_{PFR}}$ and $P_{SC_{SIR}}$, which is nearly equal to 1050 Watts in this example

In addition, the required energy rating of the SC is determined by adopting the method of Three Point Linearization [18]. The corresponding theoretical expression is given in (3), which calculates the required $E_{SC_{max}}$ to be 7,875 Jules.

$$E_{SC_{max}} = \frac{P_{PV_{avl}}\{Area\ \text{under PFR} - 2H_H k_{UF}(F_{off} - F_{nom})\}}{F_{nom} k_{UF} \beta} = 7875\ Jules \quad (3)$$

Where, β is the depth of discharge for the SC and is considered here to be 80 %. For more details on the calculation of area under PFR, please see [18].

The final part of this section is to find out the number of commercially available SC modules (N_{SC}) required to meet the calculated power and energy requirement. Here, the SC model no: BMOD0058 E016 B02 (58 F, 16 V and 170 A peak) has been assumed [18].

From the estimated $E_{SC_{max}}$, we can derive an expression as shown in (4), which implies that two SC modules are required to be connected in series to meet the energy demand.

$$N_{SC} = \left\lceil \frac{2E_{SC_{max}}}{C_{SC_{nom}} {V_{SC_{nom}}}^2} \right\rceil = 2 \quad (4)$$

Where, $C_{SC_{nom}}$ and $V_{SC_{nom}}$ are capacitance and voltage rating of the individual SC module.

However, the topological configuration of the proposed TPC has one major restriction i.e. $I_{PV_{avl}}$, which plays a vital role in deciding N_{SC} as both the ES and the primary source PV come in series during the discharging mode of operation of the SC. Considering this point, the required minimum voltage rating of the SC ($V_{SC_{min}}$) can be expressed as a function of $I_{PV_{avl}}$ and $E_{SC_{max}}$ and thus the minimum $N_{SC_{min}}$ as shown in (5).

$$N_{SC_{min}} = \left\lceil \frac{V_{SC_{min}}}{V_{SC_{nom}}} \right\rceil = \left\lceil \frac{P_{SC_{max}}}{I_{PV_{avl}} V_{SC_{nom}}} \right\rceil = 3 \quad (5)$$

From (5), it can be calculated that at least three numbers of SC modules need to be connected in series to meet both the design as well as the demand aspect.

One major observation from this section is that for the calculated SC storage (three SC modules in series), the available energy is almost three times the required energy for the prescribed under-frequency events. In addition, the maximum short-term current handling capability of the SC module is also more than seven times the targeted maximum current. This is the cost of the compact triport design, which of course indicates space for further improvement in terms of better utilization of the SC modules.

V. SIMULATION AND RESULTS

This section validates the proposed concept via MATLAB Simulink simulations for both continuous frequency fluctuation as well as under-frequency events.

A. Case Study for SIR

From Fig. 3(b), it can be seen that the power demand for RoCoF response is more intense (more than 1000 W) for the range of RoCoF nearly 0.35 Hz/sec to 0.6 Hz/sec. That is why, in order to verify the SIR concept, the PVS under consideration is subjected to an test case of continuous

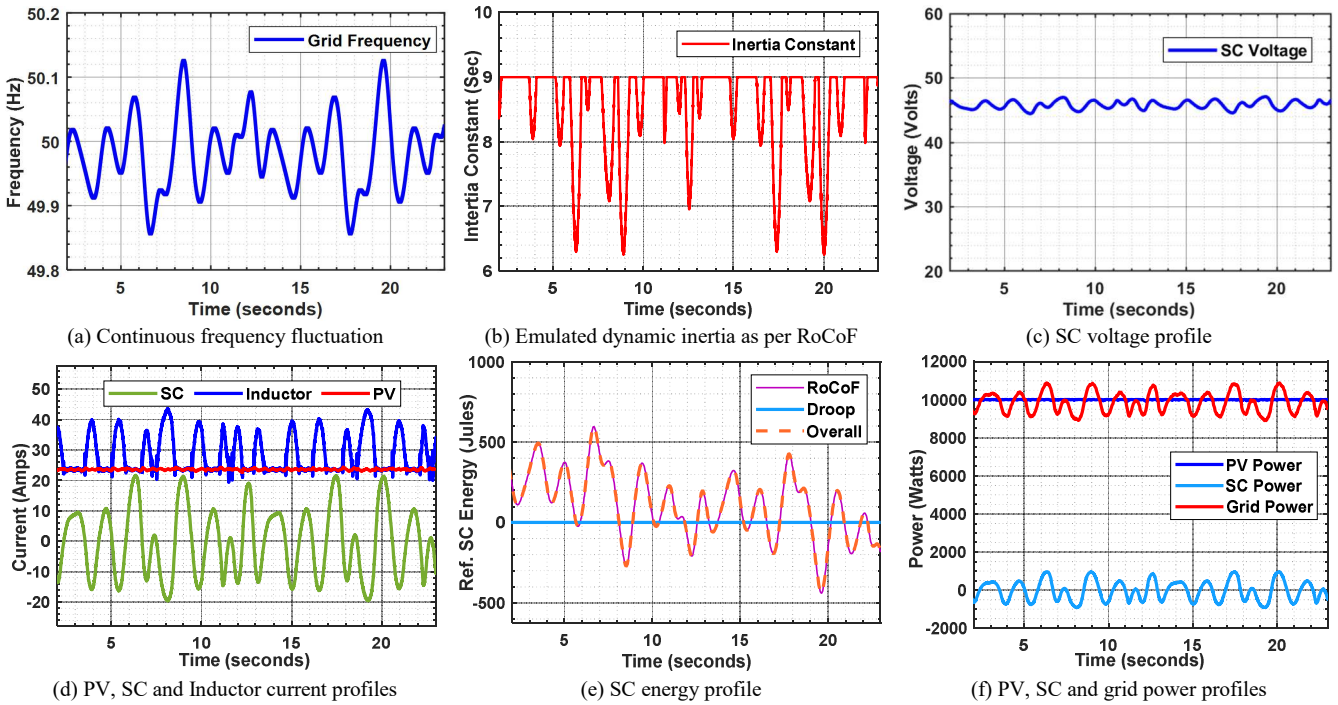

(a) Continuous frequency fluctuation (b) Emulated dynamic inertia as per RoCoF (c) SC voltage profile

(d) PV, SC and Inductor current profiles (e) SC energy profile (f) PV, SC and grid power profiles

Fig. 4. Simulation results for SIR corresponding to a case of Continuous Frequency Fluctuation event.

frequency fluctuation event with $\pm RCF_{max}$ of nearly ± 0.4 Hz/sec as a worst case for simulation based case study; in reality we expect much less steady-state frequency oscillations. The system response studied against the designed specifications in Table II and the corresponding results are shown in Fig. 4.

The following are a few observations that can be interpreted from the simulation results:

- The range of dynamic inertia emulated is between 6.2 sec to 9 sec as a function of RoCoF (Fig. 4(b)). This indicates how we can better utilize the storage capacity with the adjustable inertia constant concept.
- The net change in SC voltage in Fig. 4(c) is almost negligible over a specific period of time and it remains around the initial SC voltage of 46 V.
- Similarly, the net average SC energy in Fig. 4(e) seems negligible over a period of time, which confirms that the net energy demand for SIR is almost zero in continuous frequency fluctuation. This is why the SC capacity is not an issue for this service.
- During SC discharging period, the inductor current envelope is the same as PV current; however, during charging times, the inductor current overtakes the PV current due to Buck-Boost mode of operation (Fig. 4(d)).
- SC power pattern reflected in the Grid power profile because of SIR, subjected to grid frequency indicates the grid following mode of operation (Fig. 4(f)).

B. *Case Study for PFR*

In this case, the PVS under consideration is subject to the benchmark under-frequency event of Table I, but for two different cases of droop coefficients (Case 1: prescribed k_{UF} = 12%; Case 2: lower k_{UF} = 5%) to understand the capability and limitations of the proposed PVSC TPC configuration. The chosen values of droop coefficients are the upper and lower boundaries of the range specified by IEEE 1547-2018 [18] standard and it is always in the hand of the designer to choose a value within this range as per the targeted/available storage. Please note that the system was designed for k_{UF} =12%. and the simulation results are shown in Fig. 5.

The main observations are:

- The droop coefficient plays a vital role in draining out the energy storage. The system is perfectly capable to provide PFR for the prescribed droop coefficient of case 1 (Fig. 5(c) and (f)). However, for steeper droops like case 2, the power self-limiting nature of the proposed PVSC-TPC caps the SC current profile to the envelope of $I_{PV_{avl}}$ for the duration when the instantaneous power demand exceeds the available power. This shows that the system works fine even for the steeper droop slopes and uses more of its energy, but the power contribution is peak-shaved. This behaviour is expected due to the design, and it shows that even in this case it supports the grid to some extent.
- There is almost 7 V reduction from the initial voltage of 46 V while servicing a single under frequency event of chosen intensity for case 1 and the same is almost 13 V for case 2 (Fig. 5 (b)). This indicates that the system is still capable to serve a few back-to-back under frequency events and/or continuous frequency fluctuation (although with lower capabilities).
- The part of the power and energy demand corresponding to RoCoF response are the same for the two cases in Fig. 5(d)-(e); the difference in the overall power and energy demand is essentially due to the droop coefficients.
- The generated SC power in Fig. 5(f) is successfully shared with the grid in addition to the generated PV power because of PFR operation.

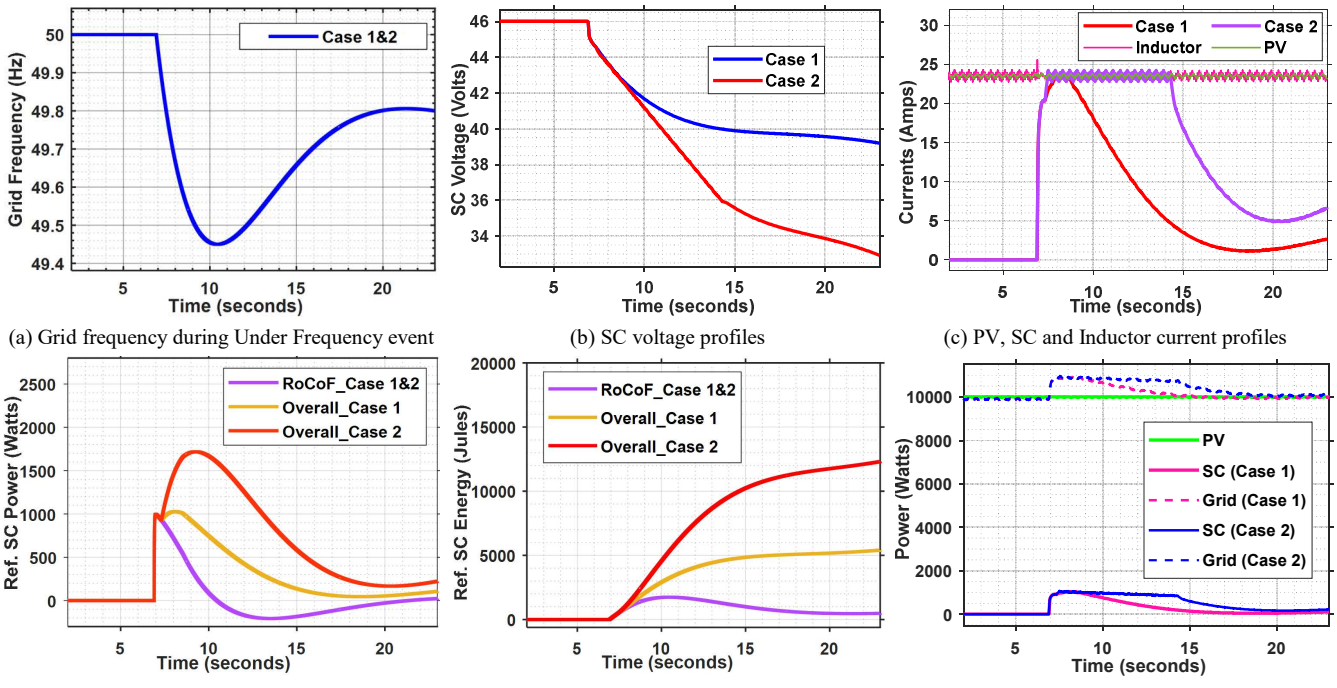

(a) Grid frequency during Under Frequency event

(b) SC voltage profiles

(c) PV, SC and Inductor current profiles

(d) Reference SC power profiles

(e) Reference SC energy profiles

(f) PV, SC and grid power profiles

Fig. 5. Simulation results for PFR corresponding to a couple of cases of Under Frequency events.

VI. Conclusion

This paper presents a simple novel single-magnetics compact multiport topology to integrate a very low voltage SC storage with a high voltage PVS without the need of a high gain converter. The main objective is to address power-intensive frequency response services for grid support with just an additional cost of almost 300 USD for a 10 kW PV inverter. Yet, the modular structure of the proposed topology has the capability to extend its application from few kWp rooftop installations to even few MWp-level solar parks.

The proposed control helps in performing the SC power control using a novel single PI controller based approach along with the PV MPPT control. The SC stage will come into picture only when there is a frequency event without hampering the regular PV MPPT operation. However, the sizing section of this paper shows that this topology needs almost 33% larger storage compared to existing works on this topic [18]. The limitation is due to the topological configuration, which brings the SC in series with PV during the time of discharge and hence limits its power discharging capability. Nevertheless, there is no limitation during the time of charging of the SC. This indicates room for further improvement of this topology for better utilization of the SCs.

Acknowledgement

This work was financially supported by DST, Govt. of India and EU's Horizon 2020 Research and Innovation Program through the RE-EMPOWERED Project under Grant Agreement No 101018420 and "India- EU Joint Call on Integrated Local Energy Systems" respectively. This work is also assisted by the Royal Academy of Engineering under the Engineering for Development Research Fellowship scheme (number RF\201819\18\86), Govt. of UK.

References

[1] Capacity-and-Generation. Available online: https://www.irena.org/Statistics/View-Data-by-Topic/Capacity-and-Generation (accessed on 2 July 2020)

[2] R. Rajan, M. F. Francis, Y. Yang, "Primary frequency control techniques for large-scale PV-integrated power systems: A review," Renew. Sustain. Energy Rev. vol. 144, pp. 1364–0321, 2021.

[3] B. Hartmann, I. Vokony, I. Táczi, "Effects of decreasing synchronous inertia on power system dynamics—Overview of recent experiences and marketisation of services," Int. Trans. Electr. Energy Syst., 29, 2019.

[4] Black System South Australia 28 September 2016—Final Report. Available online: http://www.aemo.com.au/-/media/Files/Electricity/NEM/Market_Notices_and_Events/Power_System_Incident_Reports/2017/Integrated-Final-Report-SA-Black-System-28-September-2016.pdf (accessed on 12 July 2021).

[5] H. Ibrahim, A. Ilinca, J. Perron, "Energy storage systems—Characteristics and comparisons," Renew. Sustain. Energy Rev., vol. 12, pp. 1221–1250, 2008.

[6] G. Delille, B. François, G. Malarange, "Dynamic frequency control support: A virtual inertia provided by distributed energy storage to isolated power systems," In Proceedings of the 2010 IEEE PES Innovative Smart Grid Technologies Conference Europe (ISGT Europe), Gothenburg, Sweden, pp. 1–8, 11–13 October 2010.

[7] M. M. Agha, A. Hajar, "A new approach for optimal sizing of battery energy storage system for primary frequency control of islanded Microgrid," Int. J. Electr. Power Energy Syst., vol. 54, pp. 325–333, 2014.

[8] K. Tam, P. Kumar, M. Foreman, "Enhancing the utilization of photovoltaic power generation by superconductive magnetic energy storage," IEEE Trans. Energy Convers., vol. 4, pp. 314–321, 1989.

[9] D. Sutanto, K. W. E. Cheng, "Superconducting magnetic energy storage systems for power system applications," In Proceedings of the International Conference on Applied Superconductivity and Electromagnetic Devices, Chengdu, China, 25–27 September 2009.

[10] D. Lee, L. Wang, "Small-Signal Stability Analysis of an Autonomous Hybrid Renewable Energy Power Generation/Energy Stor-age System Part I: Time-Domain Simulations," IEEE Trans. Energy Convers., vol. 23, pp. 311–320, 2008.

[11] P. C. Sekhar, S. Mishra, "Storage Free Smart Energy Management for Frequency Control in a Diesel-PV-Fuel Cell-Based Hybrid AC Microgrid," IEEE Trans. Neural Netw. Learn. Syst., vol. 27, pp. 1657–1671, 2016.

[12] A. Sangwongwanich, Y. Yang, F. Blaabjerg, D. Sera, "Delta Power Control Strategy for Multistring Grid-Connected PV Invert-ers," IEEE Trans. Ind. Appl., vol. 53, pp. 3862–3870, 2017.

[13] P. P. Zarina, S. Mishra, P. C. Sekhar, "Exploring frequency control capability of a PV system in a hybrid PV-rotating machine-without storage system," Int. J. Electr. Power Energy Syst., vol. 60, pp. 258–267, 2014.

[14] D. Bazargan, B. Bahrani, S. Filizadeh, "Reduced Capacitance Battery Storage DC-Link Voltage Regulation and Dynamic Im-provement Using a Feedforward Control Strategy," IEEE Trans. Energy Convers., vol. 33, pp. 1659–1668, 2018.

[15] K. Guo, Y. Tang, J. Fang, "Exploration of the Relationship Between Inertia Enhancement and DC-Link Capacitance for Grid-Connected Converters," In Proceedings of the IEEE 4th Southern Power Electronics Conference (SPEC), Singapore, 10–13 De-cember 2018.

[16] M. Jami, Q. Shafiee, M. Gholami, B. Hassan, "Control of a super-capacitor energy storage system to mimic inertia and transient response improvement of a direct current micro-grid," J. Energy Storage, vol. 32, pp. 101788, 2020.

[17] T. Monai, I. Takano, H. Nishikawa, Y. Sawada, "A collaborative operation method between new energy-type dispersed power supply and EDLC," IEEE Trans. Energy Convers., vol. 19, pp. 590–598, 2004.

[18] S. Karpana, E. Batzelis, S. Maiti, C. Chakraborty, "PV-Supercapacitor Cascaded Topology for Primary Frequency Responses and Dynamic Inertia Emulation," Energies, vol. 14. pp. 8347, 2021.

[19] R. Faraji, L. Ding, T. Rahimi, M. Kheshti, M. R. Islam, "Soft-Switched Three-Port DC-DC Converter with Simple Auxiliary Circuit," IEEE Access, vol. 9, pp. 66738–66750, 2021.

[20] J. Wang, K. Sun, C. Xue, T. Liu, Y. Li, "Multi-Port DC-AC Converter with Differential Power Processing DC-DC Converter and Flexible Power Control for Battery ESS Integrated PV Systems," IEEE Trans. Ind. Electron, early access, 2021.

[21] S. J. Al-Chlaihawi, "Comparative study of the multiport converter used in renewable energy systems," In Proceedings of the 2016 International Conference on Applied and Theoretical Electricity (ICATE), Craiova, Romania, 6–8 October 2016.

[22] M. C. Mira, Z. Zhang, K. L. Jørgensen, M. A. E. Andersen, "Fractional Charging Converter with High Efficiency and Low Cost for Electrochemical Energy Storage Devices," IEEE Trans. Ind. Appl., vol. 55, pp. 7461–7470, 2019.

[23] V. P. Anees, I. Biswas, K. Chatterjee, D. Kastha, P. Bajpai, "Isolated Multiport Converter for Solar PV Systems and Energy Storage Systems for DC Microgrid," In Proceedings of the 2018 15th IEEE India Council International Conference (INDICON), Coimbatore, India, 16–18 December 2018.

[24] X. Qi, D. Zhang, X. Pan and M. Fang, "A Coupled Inductors Based High Gain Non-Isolated Three-Port DC-DC Converter," IEEE International Power Electronics and Application Conference and Exposition (PEAC), pp. 1-6, 2018.

[25] G. Zhou, Q. Tian and L. Wang, "Soft-Switching High Gain Three-Port Converter Based on Coupled Inductor for Renewable Energy System Applications," IEEE Transactions on Industrial Electronics, vol. 69, no. 2, pp. 1521-1536, Feb. 2022.

[26] P. Kolahian, H. Tarzamni, A. Nikafrzoo, M. Hamzeh, "Multi-port DC–DC converter for bipolar medium voltage DC micro-grid applications," IET Power Electron., vol. 12, pp. 1841–1849, 2019.

[27] S. Nagarjun, D. Debnath and C. Chakraborty, "Buck-Boost Buck CCM-DCM Converter for PV Based DC Standalone System," IEEE International Conference on Power Electronics, Drives and Energy Systems (PEDES), pp. 1-6, 2018.

[28] M. Uno,K. Sugiyama, "Switched Capacitor Converter Based Multiport Converter Integrating Bidirectional PWM and Series-Resonant Converters for Standalone Photovoltaic Systems," IEEE Trans. Power Electron., vol. 34, pp. 1394–1406, 2019.